

# Preparation, characterization and heterogeneous catalytic applications of GO/Fe<sub>3</sub>O<sub>4</sub>/HPW nanocomposite in chemoselective and green oxidation of alcohols with aqueous H<sub>2</sub>O<sub>2</sub>

Kamran Darvishi | Kamal Amani  | Manuchehr Rezaei

Department of Chemistry, Faculty of Sciences, University of Kurdistan, P.O. Box 6617715175, Sanandaj, Iran

## Correspondence

Kamal Amani, Department of Chemistry, Faculty of Sciences, University of Kurdistan, P.O. Box 6617715175, Sanandaj, Iran.  
Email: amani\_71454@yahoo.com

Graphene oxide-Fe<sub>3</sub>O<sub>4</sub>-NH<sub>3</sub><sup>+</sup>H<sub>2</sub>PW<sub>12</sub>O<sub>40</sub><sup>-</sup> magnetic nanocomposite (GO/Fe<sub>3</sub>O<sub>4</sub>/HPW) was prepared by linking amino-functionalized Fe<sub>3</sub>O<sub>4</sub> nanoparticles (Fe<sub>3</sub>O<sub>4</sub>-NH<sub>2</sub>) on the graphene oxide (GO), and then grafting 12-tungstophosphoric acid (H<sub>3</sub>PW<sub>12</sub>O<sub>40</sub>) on the graphene oxide-magnetite hybrid (GO-Fe<sub>3</sub>O<sub>4</sub>-NH<sub>2</sub>). The obtained GO/Fe<sub>3</sub>O<sub>4</sub>/HPW nanocomposite was well characterized with different techniques such as FT-IR, TEM, SEM, XRD, EDX, TGA-DTA, AGFM, ICP and BET measurements. The used techniques showed that the graphene oxide layers were well prepared and the various stages of preparation of the GO/Fe<sub>3</sub>O<sub>4</sub>/HPW nanocomposites successfully completed. This new nanocomposite displayed excellent performance as a heterogeneous catalyst in the oxidation of alcohols with H<sub>2</sub>O<sub>2</sub>. The as-prepared GO/Fe<sub>3</sub>O<sub>4</sub>/HPW catalyst was more stable and recyclable at least five times without significantly reducing its catalytic activity.

## KEYWORDS

alcohol oxidation, Fe<sub>3</sub>O<sub>4</sub> nanoparticles, GO/Fe<sub>3</sub>O<sub>4</sub>/HPW nanocomposite, graphene oxide, H<sub>3</sub>PW<sub>12</sub>O<sub>40</sub>

## 1 | INTRODUCTION

Over the last few decades, the use of heteropoly acids (HPAs) and polyoxometalates (POMs) as catalyst in chemical reactions has become increasingly important and their application has been reviewed.<sup>[1-5]</sup> The benefits of many heteropoly acids are their use in catalyzing various chemical reactions as Bronsted acid. Polyoxometalates have reversible multi-electron redox behavior that makes them potential catalysts in oxidative reactions in homogeneous or heterogeneous conditions.<sup>[2]</sup> Moreover, by changing the POM structure, their chemical properties can be customized. Keggin-type heteropoly acids such as H<sub>3</sub>PW<sub>12</sub>O<sub>40</sub>, H<sub>3</sub>PMo<sub>12</sub>O<sub>40</sub> or H<sub>4</sub>SiW<sub>12</sub>O<sub>40</sub> are the most popular and the most efficient. HPAs are soluble in polar and oxidative media and therefore not easily

recyclable in chemical reactions. Usually, they are used in non-polar solvents as a heterogeneous catalyst but in these conditions they also have a low surface area (<10 m<sup>2</sup>/g).<sup>[1-5]</sup>

To solve the above mentioned problems, two heterogenization methods have been proposed: (i) exchange of heteropoly acid protons with bulk organic and inorganic cations which can reduce the solubility and increase their surface area, (ii) immobilization of heteropoly acids and polyoxometalates on suitable solid supports with high surface area.<sup>[3]</sup> It should be emphasized that by heterogenization of HPAs, their activity is decreased relative to the initial catalyst and homogeneous conditions and the catalyst is probably leached out from the support surface in catalyst recycling. Therefore, the covalent or ionic nature of the interaction between HPA

and the support surface is significant and affects the physicochemical properties, catalytic activity, and leaching of the active species.<sup>[6–20]</sup> Various insoluble supports have been used for immobilization of HPAs such as silica, titana, alumina, zirconia, carbon, cellulose, zeolites and clays, metal oxides, organic materials and metal-organic frameworks.<sup>[2,3,5–19]</sup>

Graphene oxide (GO) has a special single monolayer structure with aromatic and aliphatic regions, and various functional groups such as hydroxyl, epoxy, carboxylic and carbonyl groups are located on the surface of each layer. Usually, graphite oxide is prepared from the oxidation of graphite and has extensive applications in biosensors,<sup>[20,21]</sup> imaging,<sup>[22,23]</sup> membrane,<sup>[24–29]</sup> and electrocatalysis fields.<sup>[22,24,30–32]</sup> Recently, the functionalization of graphene oxide has attracted considerable attention and various methods have been used for this purpose in which organic groups are deposited on the surface of graphite oxide through covalent bonding usually by bonding with carboxylic acid groups, forming amides and esters groups or by nucleophilic attack on the epoxy rings.<sup>[30,33–37]</sup> In the recent past, in order to utilize its high surface area, graphene and graphene oxide have been used as a support and many types of nanoparticles are immobilized or deposited onto them. Some examples of this type of hybrid composite are GO/enzymes,<sup>[20]</sup> GO/Fe<sub>3</sub>O<sub>4</sub>,<sup>[38–40]</sup> Au-nanoparticle/ polyoxometalate/graphene nanohybrid,<sup>[21]</sup> GO/polyoxometalate composite film,<sup>[41]</sup> and graphene/HPA.<sup>[42]</sup> The decoration with magnetic nanoparticles is particularly interesting because magnetic graphene oxide is easily separated from the reaction medium using an external magnet.

Magnetic nanoparticles (MNPs) are widely used as support in catalytic systems due to easy separation and reuse. The main disadvantage of MNPs is their low surface area. Thus, to fix this deficiency, MNPs are often placed in a composite structure alongside particles with a high surface area. GO sheets with an excellent surface area and easy connection are ideal options. Several methods have been used to situate the MNPs on the surface of GO sheets, such as (i) formation of the MNPs on the surface of GO layers and (ii) linking of pre-prepared MNPs through covalent bonds to GO.<sup>[21,38–42]</sup>

Oxidation of alcohols is one of the more important and popular reactions in organic chemistry and so far dozens of articles have been reported in this field. The oxidation of alcohols in accordance with the principles of green chemistry is limited to some environmentally benign oxidants including hydrogen peroxide and molecular oxygen. Various methods that use hydrogen peroxide as oxidizing agents in the presence of heteropoly acids and polyoxometalates to oxidize primary and secondary

alcohols to its corresponding carbonyl compounds have been reported in the literature.<sup>[4,11–18,43–59]</sup> The mechanism of the effect of heteropoly acids and polyoxometalates is well known in catalyzing of oxidation reactions with hydrogen peroxide, and suggests the formation of an active species: Ishii–Venturello complex {PO<sub>4</sub>[WO(O<sub>2</sub>)<sub>2</sub>]<sub>4</sub>}<sup>3–</sup>.<sup>[60,61]</sup>

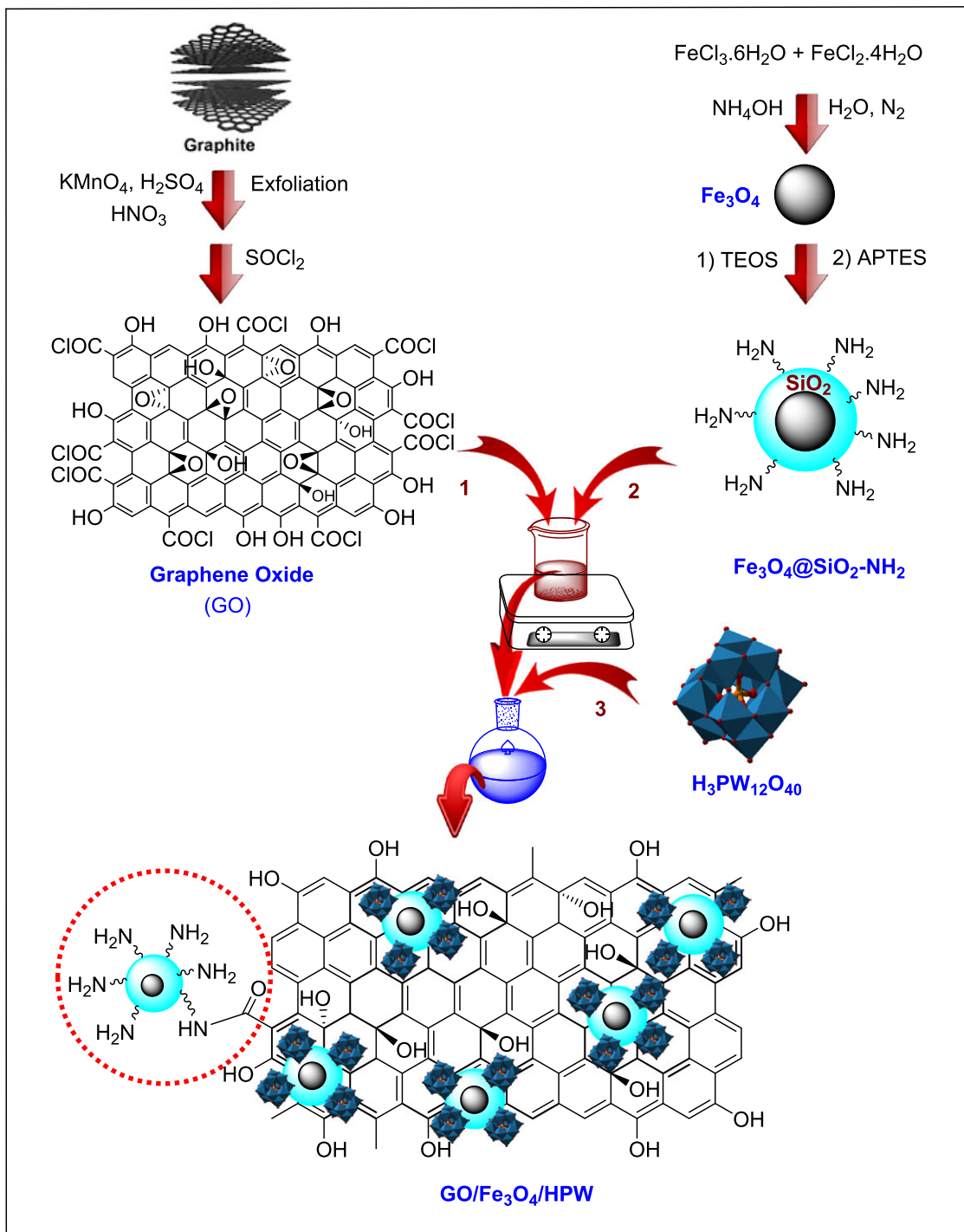
Some previous reports have several defects as follows: (i) the use of the catalyst in homogeneous conditions which makes the process of separation and reuse of the catalyst more difficult; (ii) the need for centrifuge or filtering to separation of catalyst which are not simple processes; (iii) over-oxidation of alcohols to the corresponding carboxylic acids; (iv) the use of volatile and harmful organic solvents; (v) the need for rough conditions to carry out oxidation reaction such as high temperature, very long reaction time, high concentration of H<sub>2</sub>O<sub>2</sub>; (vi) the weak linking of HPAs and POMs onto carrier which leads to leaching out of HPA and POM during the oxidation process. We have attempted to develop and introduce a new catalytic system based on H<sub>3</sub>PW<sub>12</sub>O<sub>40</sub> to eliminate these deficiencies.

Therefore, with regard to the cases cited above and in the continuation of our activities in the synthesis of nanoparticles and nanocomposites and their applications in organic synthesis,<sup>[9,62,63]</sup> we planned to design and synthesize GO/Fe<sub>3</sub>O<sub>4</sub>/HPW nanocomposite as a catalytic system with the hope that this system has unique catalytic properties of heteropoly acids and high surface area to have a heterogeneous condition which allows high stability and easy separation from the reaction mixture (Scheme 1). In continuation, we employed a facile and efficient approach for chemoselective oxidation of alcohols to corresponding aldehydes or ketones catalyzed by GO/Fe<sub>3</sub>O<sub>4</sub>/HPW nanocomposite with H<sub>2</sub>O<sub>2</sub> under organic solvent-free conditions.

## 2 | EXPERIMENTAL SECTION

### 2.1 | Materials

All chemicals were purchased from Merck chemical company with no further purification. Fourier transforms infrared spectra were recorded using FT-IR Bruker (TENSOR 27) spectrometer and KBr plates. Scanning electron micrographs (SEM) and energy-dispersive X-ray spectroscopy (EDX) of the samples were taken with FE-SEM from TSCAN Company. The magnetic properties of the studied samples were measured by an alternating gradient force magnetometer (AGFM) at room temperature. Thermal analyses (TGA-DTA) were performed using a Linseis STA PT 1000 instrument at room temperature to 600 °C. Melting points of solid samples were measured and



**SCHEME 1** The strategy for the synthesis of the GO/Fe<sub>3</sub>O<sub>4</sub>/HPW nanocomposite

determined with an electrothermal 9100 apparatus. X-ray diffraction (XRD) pattern of the product was carried out with a X'Pert Pro Philips X-ray diffractometer with Cu K $\alpha$  radiation, and the scan range (2  $\theta$ ) was from 10° to 80°. The transmission electron microscopy (TEM) images were recorded by a Philips microscope (EM 208, Tokyo, Japan) operating at 100 kV. The Brunauer-Emmett-Teller (BET) surface area was obtained by applying the BET equation and  $P/P_0 = 0.305$  to the adsorption data,

respectively. The amount of Fe, Si, and W elements was obtained using the ICP-OES (Varian, 730-ES). All the reported yields for the reaction products are the isolated yields.

## 2.2 | Preparation of graphene oxide (GO)

Graphene oxide (GO) was made from graphite by the modified Hummers method.<sup>[64,65]</sup>

### 2.3 | Preparation of acid chlorides of graphene oxide (GOCl)

GOCl was prepared according to the previously reported method.<sup>[66]</sup>

### 2.4 | Preparation of silica-coated Fe<sub>3</sub>O<sub>4</sub> MNPs (Fe<sub>3</sub>O<sub>4</sub>@SiO<sub>2</sub>)

Fe<sub>3</sub>O<sub>4</sub>@SiO<sub>2</sub> nanoparticles were prepared following a method reported previously in the literature.<sup>[9]</sup>

### 2.5 | Preparation of NH<sub>2</sub>-functionalized Fe<sub>3</sub>O<sub>4</sub>@SiO<sub>2</sub> MNPs (Fe<sub>3</sub>O<sub>4</sub>-NH<sub>2</sub>)

Fe<sub>3</sub>O<sub>4</sub>-NH<sub>2</sub> nanoparticles were prepared with surface modification of Fe<sub>3</sub>O<sub>4</sub>@SiO<sub>2</sub> using APTES in ethanol.<sup>[67]</sup>

### 2.6 | Preparation of the graphene oxide-Fe<sub>3</sub>O<sub>4</sub> MNPs (GO-Fe<sub>3</sub>O<sub>4</sub>)

GO-Fe<sub>3</sub>O<sub>4</sub> was prepared according to the method described in the literature.<sup>[66]</sup>

### 2.7 | Preparation of GO-Fe<sub>3</sub>O<sub>4</sub>-NH<sub>3</sub><sup>+</sup>H<sub>2</sub>PW<sub>12</sub>O<sub>40</sub><sup>-</sup> nanocomposite (GO/Fe<sub>3</sub>O<sub>4</sub>/HPW)

100 mg of GO-Fe<sub>3</sub>O<sub>4</sub> MNPs was dispersed in 5 ml of deionized water and ultrasonicated for 30 min. Then, a solution of H<sub>3</sub>PW<sub>12</sub>O<sub>40</sub>.nH<sub>2</sub>O (200 mg) dissolved in 2 ml deionized water was added dropwise into the solution and ultrasonicated for a further 30 min and the mixture stirred for 24 h at room temperature. Finally, the formed GO/Fe<sub>3</sub>O<sub>4</sub>/HPW nanocomposite was magnetically separated and washed twice with water and dried at 60 °C.

### 2.8 | Oxidation of alcohols to the corresponding aldehydes or ketones by H<sub>2</sub>O<sub>2</sub>

2 ml of H<sub>2</sub>O<sub>2</sub> (10%, about 5 mmol) with 1 mmol of the alcohol and 20 mg of the catalyst was charged into a round-bottomed flask. The resultant mixture was stirred at 70 °C. The progress of the reaction was followed by thin-layer chromatography (TLC). After the completion of the reaction, the GO/Fe<sub>3</sub>O<sub>4</sub>/HPW was separated using the magnet and the reaction mixture was extracted with ether (3×5 ml). After drying the organic phase and purifying the products by chromatographic methods, the products were identified by various spectroscopic methods. The solid catalyst was washed three times with ethanol and then dried under vacuum for subsequent use.

## 3 | RESULTS AND DISCUSSION

As can be seen in Scheme 1 and in the 'Experimental Section', our magnetic catalytic system was prepared in several steps. The structure of the synthesized catalyst was then characterized by different physicochemical techniques such as FT-IR, XRD, EDX, FE-SEM, TEM, TGA, BET, ICP and AGFM.

### 3.1 | Fourier Transform Infrared Spectroscopy (FT-IR)

Figure 1 shows FT-IR spectra for graphite, GO, GOCl, Fe<sub>3</sub>O<sub>4</sub>, Fe<sub>3</sub>O<sub>4</sub>@SiO<sub>2</sub>, Fe<sub>3</sub>O<sub>4</sub>-NH<sub>2</sub>, GO-Fe<sub>3</sub>O<sub>4</sub>, H<sub>3</sub>PW<sub>12</sub>O<sub>40</sub> and GO/Fe<sub>3</sub>O<sub>4</sub>/HPW. In the FT-IR spectra of GO, the peaks at 1729 and 1615 cm<sup>-1</sup> is related to stretching vibration of C=O and C=C bonds, respectively, and a very broad peak in the range of 3500-2500 cm<sup>-1</sup> is attributed to the stretching vibrations of O-H bonds of acidic and alcoholic groups (Figure 1, b). The peaks at 1220, 1051 and 991 cm<sup>-1</sup> correspond to asymmetric and symmetric vibrations of the epoxy ring and the stretching vibration of C-O in the order mentioned.<sup>[68]</sup>

In the curve of Fe<sub>3</sub>O<sub>4</sub> NPs (Figure 1, d), the peak at about 570 cm<sup>-1</sup> is ascribed to Fe-O stretching vibration.<sup>[69]</sup> In FT-IR spectrum of silica-coated MNPs (Figure 1, e), the peaks intensity of Fe-O bond is decreased and the sharp band at about 1063 cm<sup>-1</sup> is attributed to Si-O-Si asymmetric stretching vibration indicating the survival of a SiO<sub>2</sub> layer around the Fe<sub>3</sub>O<sub>4</sub> nanoparticles.<sup>[70]</sup>

In f and g curves, the peak of about 3430 cm<sup>-1</sup> is attributed to N-H stretching, but this peak can interfere with a peak of O-H stretching absorbance. Furthermore, the peaks of N-H bending at 1629 cm<sup>-1</sup> for Fe<sub>3</sub>O<sub>4</sub>-NH<sub>2</sub> is clearly observed (Figure 1, f and g).<sup>[70]</sup> In the FT-IR spectrum of GO-Fe<sub>3</sub>O<sub>4</sub> hybrid (Figure 1, g), two peaks at around 1648 and 1600 cm<sup>-1</sup> are related to C=O bond of the amide group and C=C bond in the graphene layer, respectively. The peak at 3430 cm<sup>-1</sup> is concern the stretching vibration of O-H and N-H bonds that overlap.<sup>[66]</sup> In FT-IR spectrum of H<sub>3</sub>PW<sub>12</sub>O<sub>40</sub> four characteristic vibration peaks at 1081 (P-O), 985 (W=O), 890 and 795 (W-O-W) cm<sup>-1</sup> are shown. Compared to the starting Keggin unit, the peak at 1081 cm<sup>-1</sup> overlap with Si-O-Si stretching vibration but new peaks at 979, 893 and 810 cm<sup>-1</sup> are observed on FT-IR spectrum of GO/Fe<sub>3</sub>O<sub>4</sub>/HPW (Figure 1, i) indicating that H<sub>3</sub>PW<sub>12</sub>O<sub>40</sub> was anchored to the GO-Fe<sub>3</sub>O<sub>4</sub> hybrid successfully.<sup>[71]</sup>

### 3.2 | Thermogravimetric analysis (TGA)

The thermal stability of GO, GO-Fe<sub>3</sub>O<sub>4</sub>, and the GO/Fe<sub>3</sub>O<sub>4</sub>/HPW nanocomposite were analyzed by TGA.

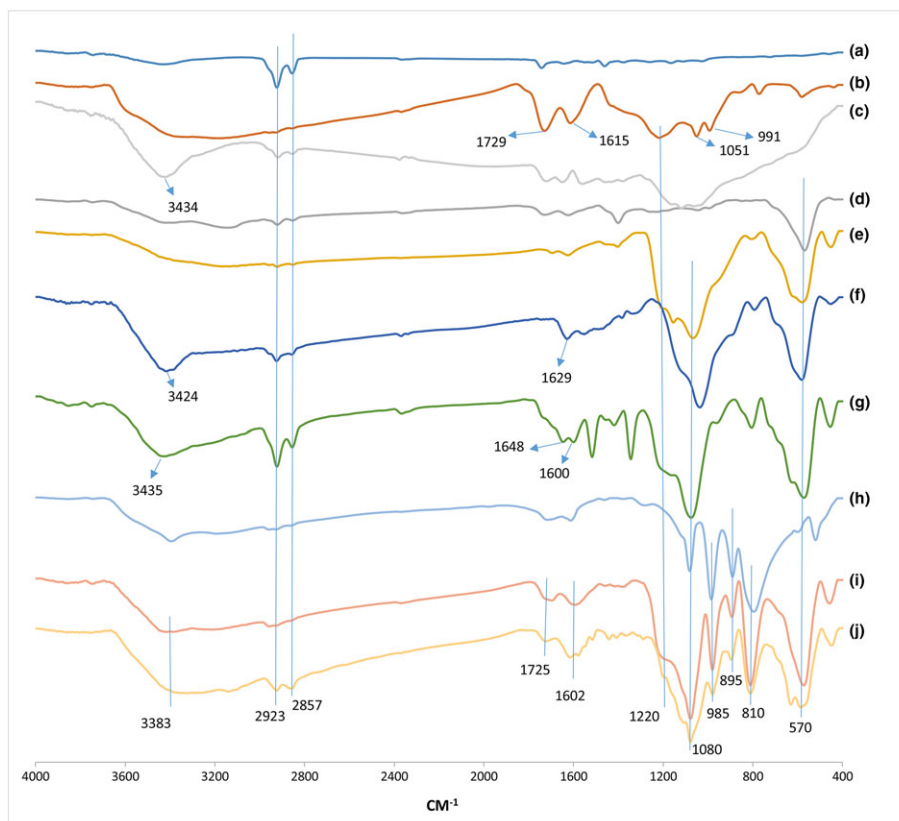


**FIGURE 1** FT-IR spectra of (a) G, (b) GO, (c) GOCl, (d)  $\text{Fe}_3\text{O}_4$ , (e)  $\text{Fe}_3\text{O}_4@SiO_2$ , (f)  $\text{Fe}_3\text{O}_4\text{-NH}_2$ , (g) GO- $\text{Fe}_3\text{O}_4$  hybrid, (h)  $\text{H}_3\text{PW}_{12}\text{O}_{40}$ , (i) fresh GO/ $\text{Fe}_3\text{O}_4$ /HPW, and (j) GO/ $\text{Fe}_3\text{O}_4$ /HPW after recycling in run 5

Samples were heated under an atmosphere of  $\text{N}_2$  at rt. to  $600^\circ\text{C}$  at a heating rate of  $10^\circ\text{C}/\text{min}$  (Figure 2). Graphene oxide was thermally unstable and even at less than  $100^\circ\text{C}$ , it began to lose moisture and thus the mass. Losing approximately 12% of the weight below  $150^\circ\text{C}$  and 65% in the temperature range of  $150\text{--}266^\circ\text{C}$  indicates extensive oxidation of graphene oxide. GO- $\text{Fe}_3\text{O}_4$  also had a weight loss of approximately 3.4% at  $200^\circ\text{C}$  and 10.5% in the range of  $200\text{--}600^\circ\text{C}$ . This illustrates that GO- $\text{Fe}_3\text{O}_4$  is more stable than GO. The TGA curve for GO/ $\text{Fe}_3\text{O}_4$ /HPW nanocomposite shows only

approximately 6.5% weight loss at  $600^\circ\text{C}$ . This demonstrates that the GO/ $\text{Fe}_3\text{O}_4$ /HPW nanocomposite has a high thermal stability.

### 3.3 | Magnetic properties

The magnetic properties were measured at room temperature as illustrated in Figure 3. The saturation magnetizations for  $\text{Fe}_3\text{O}_4$ ,  $\text{Fe}_3\text{O}_4@SiO_2$ ,  $\text{Fe}_3\text{O}_4\text{-NH}_2$  nanoparticles, GO- $\text{Fe}_3\text{O}_4$  hybrid, and GO/ $\text{Fe}_3\text{O}_4$ /HPW nanocomposite are 0.437, 0.191, 0.189, 0.175 and 0.112 M (a.u.), respectively. The magnetic property of the GO/ $\text{Fe}_3\text{O}_4$ /HPW nanocomposite was so high that it took only a few seconds to separate with the external magnet from the aqueous solution, which made it possible to recycle and reuse the catalyst.

### 3.4 | Scanning electron micrograph (SEM)

The SEM technique was used to study the morphology of GO/ $\text{Fe}_3\text{O}_4$ /HPW nanocomposite (Figure 4). The SEM images confirm the successful attachment of  $\text{Fe}_3\text{O}_4\text{-NH}_2$  and  $\text{H}_3\text{PW}_{12}\text{O}_{40}$  nanoparticles on GO surface. Regarding Figures b and c, it can be observed that graphene oxide sheets are distributed between  $\text{Fe}_3\text{O}_4\text{-NH}_2$  and  $\text{H}_3\text{PW}_{12}\text{O}_{40}$  nanoparticles and GO/ $\text{Fe}_3\text{O}_4$ /HPW

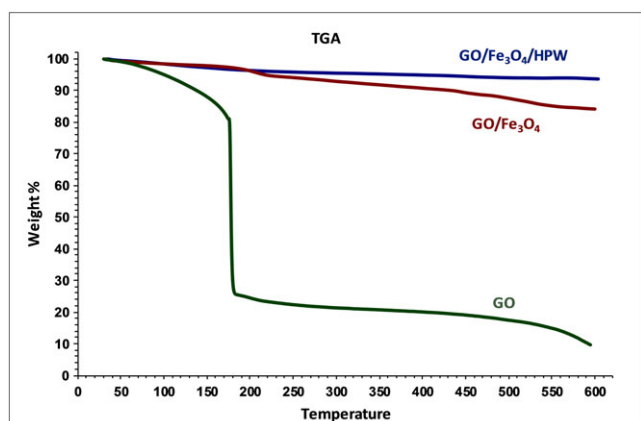


**FIGURE 2** TGA analysis of GO, GO- $\text{Fe}_3\text{O}_4$ , and GO/ $\text{Fe}_3\text{O}_4$ /HPW

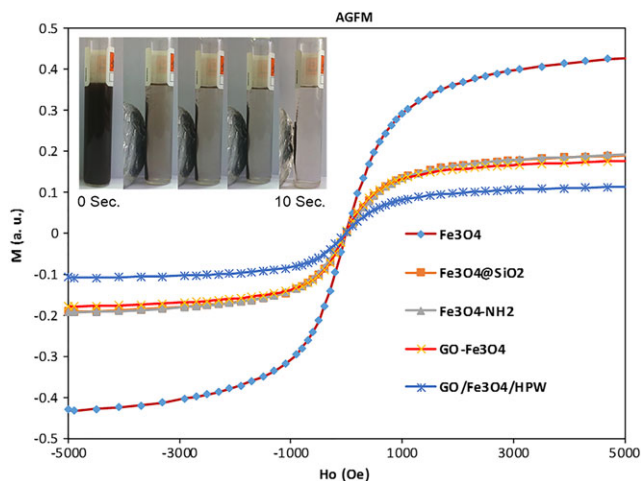


**FIGURE 3** Magnetization curves of  $\text{Fe}_3\text{O}_4$ ,  $\text{Fe}_3\text{O}_4@\text{SiO}_2$ ,  $\text{Fe}_3\text{O}_4\text{-NH}_2$ ,  $\text{GO-Fe}_3\text{O}_4$  and  $\text{GO/Fe}_3\text{O}_4/\text{HPW}$

nanocomposite are well-formed with a large amount of free space. The  $\text{Fe}_3\text{O}_4\text{-NH}_2$  nanoparticles are anchored uniformly and with a high density on the wrinkled GO layers. In particular, the pleat structure of GO may prevent the accumulation and agglomeration of  $\text{Fe}_3\text{O}_4\text{-NH}_2$  and  $\text{H}_3\text{PW}_{12}\text{O}_{40}$  particles and contribute to their better distribution.

### 3.5 | Energy dispersive X-ray analysis (EDX)

Energy dispersive X-ray analysis (EDX) of  $\text{GO/Fe}_3\text{O}_4/\text{HPW}$  nanocomposite is shown in Figure 5. The elemental analysis by the EDX recorded peaks is related to C, O, N, Fe, W, P, Si elements. Therefore, the EDX analysis confirmed the presences of expected elements in the structure of the synthesized  $\text{GO/Fe}_3\text{O}_4/\text{HPW}$  nanocomposite. The ICP analysis was used to determine the quantity of

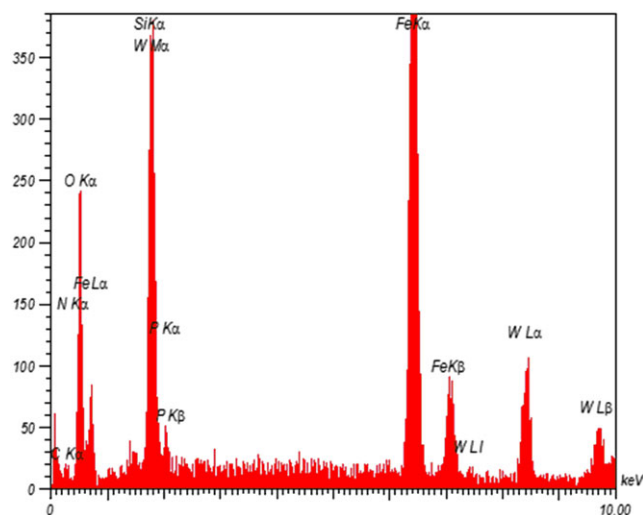


**FIGURE 5** Energy dispersive X-ray analysis (EDX) of  $\text{GO/Fe}_3\text{O}_4/\text{HPW}$

catalyst loaded. The results showed that the amount of HPA loaded on the support is 19.76%wt.

### 3.6 | X-ray diffraction (XRD)

The structures of GO,  $\text{Fe}_3\text{O}_4\text{-NH}_2$ ,  $\text{H}_3\text{PW}_{12}\text{O}_{40}$ , and  $\text{GO/Fe}_3\text{O}_4/\text{HPW}$  nanocomposite were identified by XRD technique shown in Figure 6. GO has two distinct peaks at  $2\theta = 11.5^\circ$  and  $42.3^\circ$ , and the peak removal of  $2\theta = 26.4^\circ$  indicates successful oxidation of graphite to graphene oxide by the Hummer method.<sup>[21,66,68]</sup> Diffraction peaks with  $2\theta = 30.3, 35.8, 43.4, 53.8, 57.3, 62.8, 71.3$  and  $74.3$  properly confirm the structure of  $\text{Fe}_3\text{O}_4\text{-NH}_2$ . The peak positions and relative intensities are consistent with standard XRD data for magnetite, which indicates good formation of  $\text{Fe}_3\text{O}_4$  NPs.<sup>[9]</sup>

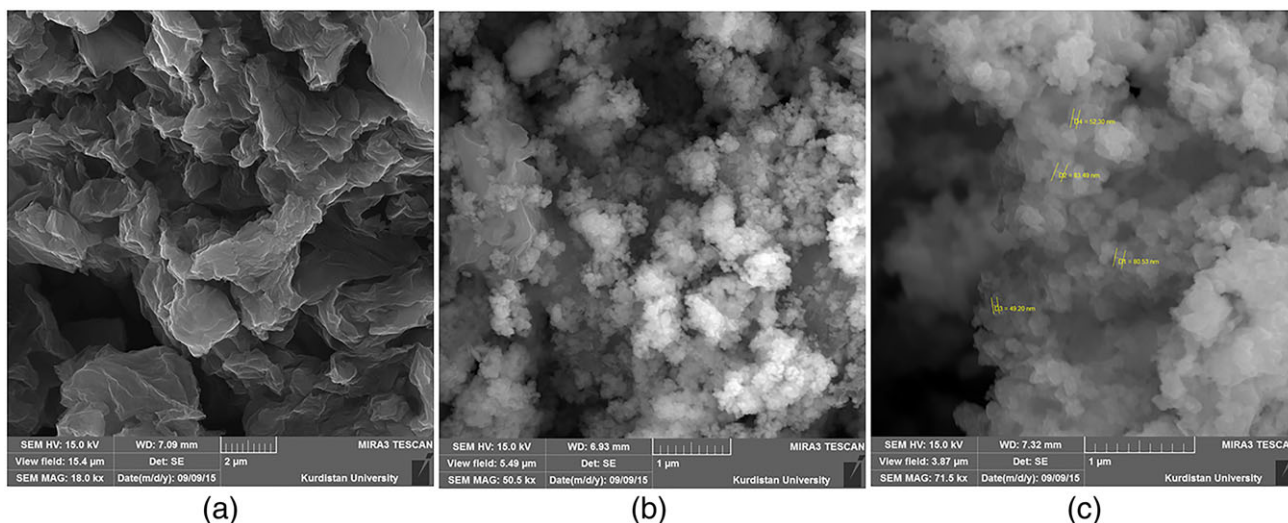


**FIGURE 4** SEM images of GO (a), and  $\text{GO/Fe}_3\text{O}_4/\text{HPW}$  (b and c)

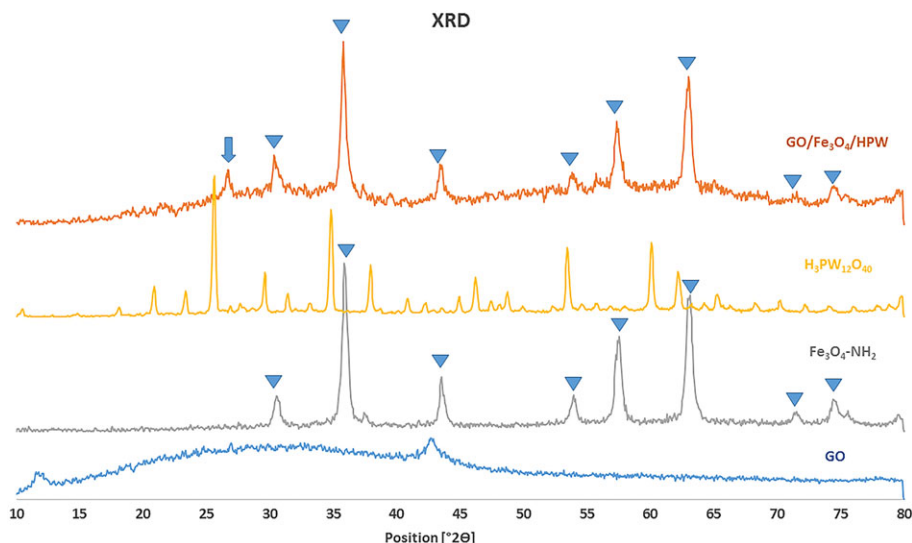


**FIGURE 6** XRD patterns of GO,  $\text{Fe}_3\text{O}_4\text{-NH}_2$ ,  $\text{H}_3\text{PW}_{12}\text{O}_{40}$  and  $\text{GO/Fe}_3\text{O}_4\text{/HPW}$

The characteristic and sharp diffraction peaks of  $\text{H}_3\text{PW}_{12}\text{O}_{40}$  which confirm its crystalline structure is not visible in  $\text{GO/Fe}_3\text{O}_4\text{/HPW}$  nanocomposite indicating the non-crystalline structure of the  $\text{H}_3\text{PW}_{12}\text{O}_{40}$  immobilized on the support. The  $\text{GO/Fe}_3\text{O}_4\text{/HPW}$  nanocomposite has inherited  $\text{Fe}_3\text{O}_4$  diffraction peaks with the same position but with a slight decrease in their intensities.<sup>[15,17,72]</sup> Diffraction peaks with  $2\theta = 26.7, 30.3, 35.7, 43.5, 53.7, 57.3, 63.0$  and  $74.4$  are registered in the XRD pattern of  $\text{GO/Fe}_3\text{O}_4\text{/HPW}$  nanocatalyst. The average size calculated for the magnetic nanoparticles from the XRD data according to the Scherrer equation are about 15.56 and 28.37 nm for the  $\text{Fe}_3\text{O}_4\text{-NH}_2$  nanoparticles and  $\text{GO/Fe}_3\text{O}_4\text{/HPW}$  nanocomposite, respectively.

### 3.7 | Transmission electron micrographs (TEM)

The morphology and particle size of the prepared  $\text{GO/Fe}_3\text{O}_4\text{/HPW}$  nanocomposites were further analyzed using TEM technique and is shown in Figure 7. The images clearly indicate the accumulation of  $\text{Fe}_3\text{O}_4$  and  $\text{Fe}_3\text{O}_4\text{-NH}_2$  nanoparticles on the wrinkled surface of GO. A large number of nanoparticles are distributed randomly on the surface and edges of the graphene sheets.<sup>[40,73]</sup>

### 3.8 | Brunauer Emmet Teller (BET)

The specific surface area of  $\text{H}_3\text{PW}_{12}\text{O}_{40}$ , graphite powder, GO, and  $\text{Fe}_3\text{O}_4\text{-NH}_2$  nanoparticles measured were approximately 5, 8.5, 492, and  $162 \text{ m}^2/\text{g}$ , respectively.<sup>[74-76]</sup> The specific surface area of the  $\text{GO/Fe}_3\text{O}_4\text{/HPW}$  nanocomposite measured was approximately  $478 \text{ m}^2 \text{ g}^{-1}$ , which is remarkably high. As expected, the specific surface area for the  $\text{GO/Fe}_3\text{O}_4\text{/HPW}$  nanocomposite was

close to the specific surface area reported for the graphene oxide. It is a fact that having such high surface area is a major advantage for the catalytic activity of this nanocomposite.

## 3.9 | Catalytic activity studies

First, to evaluate the efficiency of the catalyst, the oxidation of benzyl alcohol to benzaldehyde by hydrogen peroxide in the presence of the catalytic amount of  $\text{GO/Fe}_3\text{O}_4\text{/HPW}$  was selected as the probe reaction (Scheme 2) and the reaction conditions were optimized.

### 3.9.1 | Influence of reaction temperature and reaction time

At 25, 30, 40 °C, even after 24 hours, the reaction did not progress significantly. With the increase of the reaction temperature from 50 to 70 °C, the conversion of benzyl alcohol increased from 10% to up to 99% and the reaction time was drastically reduced to 3 hours. Increasing the reaction temperature to 80 °C would not change much in the yield of the product, but with increment the reaction temperature to 90 and 100 °C, due to over-oxidation to benzoic acid, selectivity was decreased (Figure 8).

### 3.9.2 | Influence of the amount of $\text{H}_2\text{O}_2$

In the presence of various amounts of 10% hydrogen peroxide and by considering the above-mentioned conditions, the oxidation reaction of 1 mmol benzyl alcohol to benzaldehyde occurred (Figure 9). The results revealed that the yield of benzaldehyde was positively dependent on the amounts of  $\text{H}_2\text{O}_2$ . By increasing the amount of 10%  $\text{H}_2\text{O}_2$  to 5 mmol, the conversion increased gently to 98%.

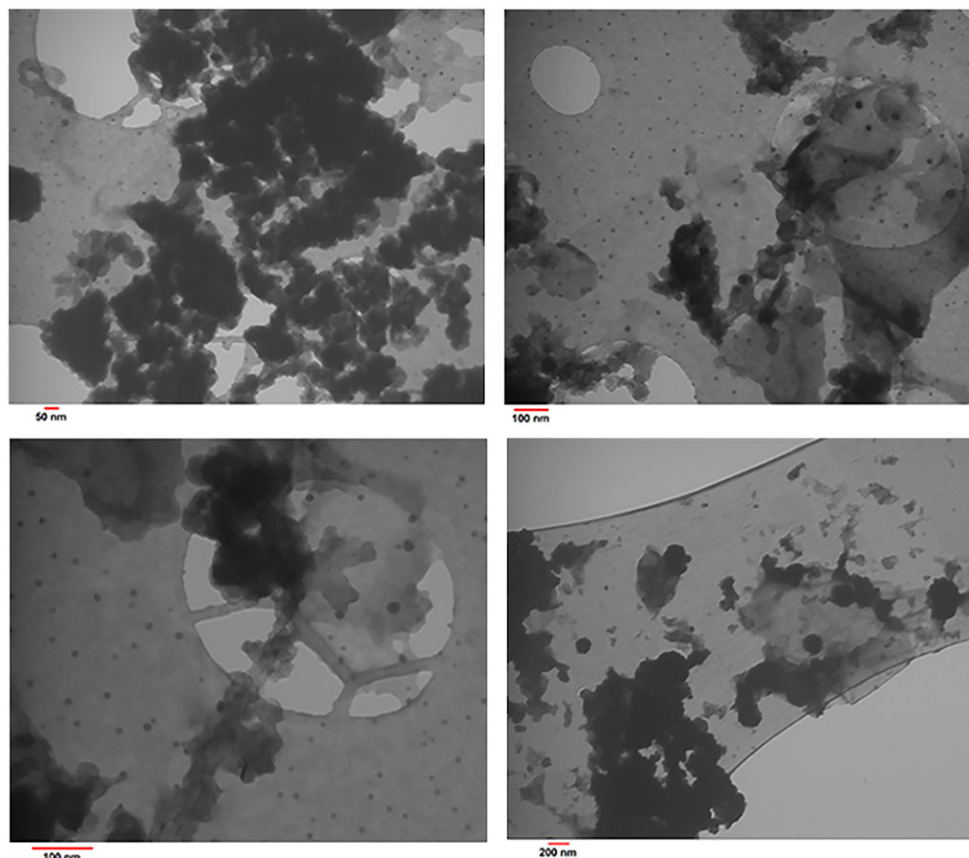
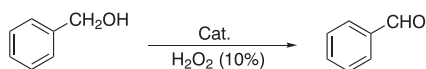


**FIGURE 7** Representative TEM images of GO/Fe<sub>3</sub>O<sub>4</sub>/HPW



**SCHEME 2** The oxidation reaction of benzyl alcohol to benzaldehyde

### 3.9.3 | Influence of the amount of catalyst

Under the above-optimized conditions, the oxidation of benzyl alcohol in the presence of 10 and 15 mg GO/Fe<sub>3</sub>O<sub>4</sub>/HPW nanocatalyst only resulted in benzaldehyde

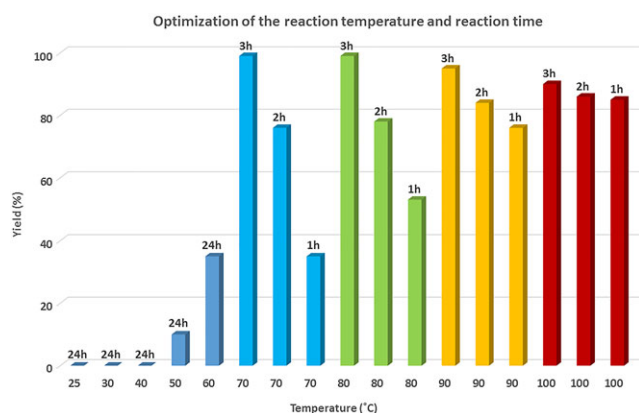


**FIGURE 8** Optimization of the reaction temperature and the reaction time in the oxidation reaction of benzyl alcohol

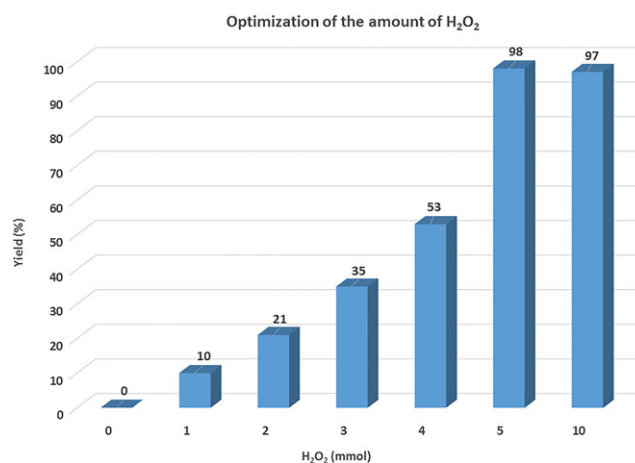


**FIGURE 9** Optimization of the amount of H<sub>2</sub>O<sub>2</sub> (mmol) in the oxidation of 1 mmol benzyl alcohol

in 20% and 63% yields, respectively. Further increasing the amount of catalyst up to 20 mg afforded the desired product in excellent yields of 98% under the same reaction conditions (Figure 10). Increasing the catalyst amount by more than 20 mg led to a slight reduction in selectivity. The oxidation of benzyl alcohol in the presence of HPW and GO-Fe<sub>3</sub>O<sub>4</sub> were also performed. The results of Table ESI-1 show that under homogeneous conditions and in

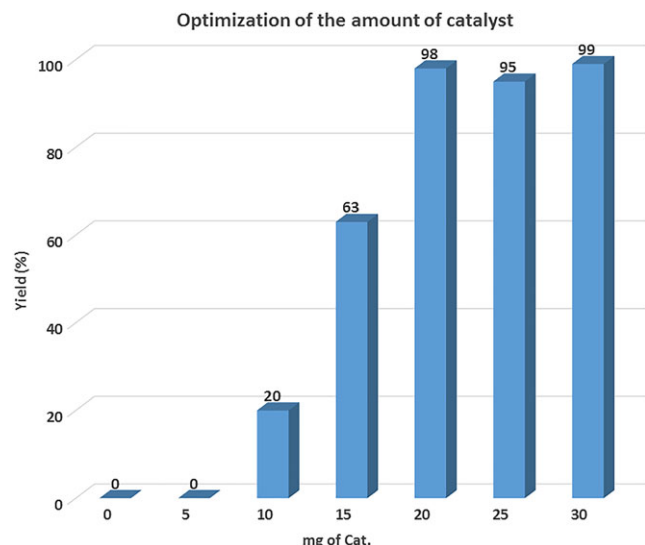


**FIGURE 10** Optimization of the amount of GO/Fe<sub>3</sub>O<sub>4</sub>/HPW (mg) in the oxidation of 1 mmol benzyl alcohol

the presence of 20 mg HPW, within 2 h, the reaction yield is 97%, while in the presence of GO-Fe<sub>3</sub>O<sub>4</sub>, within 8 h, no product is obtained. This indicates the need for acid to catalyze the oxidation reaction.

Therefore, the ideal conditions for the selective oxidation of benzyl alcohol to benzaldehyde in the present work is as follows: the oxidation of 1 mmol benzyl alcohol was carried out with 20 mg of GO/Fe<sub>3</sub>O<sub>4</sub>/HPW catalyst in the presence of 10% H<sub>2</sub>O<sub>2</sub> (5 mmol) at 70 °C and within 3 h under organic solvent-free conditions to meet the requirements of a green oxidation reaction. Interestingly, under this condition, benzyl alcohol was selectively transformed into the corresponding benzaldehyde without any detectable overoxidation to benzoic acid.

For obtaining the optimal reaction conditions, we decided to investigate the scope of GO/Fe<sub>3</sub>O<sub>4</sub>/HPW in the oxidation of various primary and secondary alcohols. The experimental results indicate that the catalytic performance of the GO/Fe<sub>3</sub>O<sub>4</sub>/HPW nanocomposite in the

**TABLE 1** Catalytic performance of the GO/Fe<sub>3</sub>O<sub>4</sub>/HPW nanocatalyst for the selective oxidation of alcohols with H<sub>2</sub>O<sub>2</sub> under optimal reaction conditions<sup>a</sup>

Entry <sup>a</sup>	Alcohol	Product	Time (h)	Yield <sup>b</sup> (%)	Selectivity <sup>c</sup> (%)
1			3	99	100
2			1.30	100	100
3			2	99	100
4			4	94	100
5			9	70	100
6			7	90	100
7			6	85	100
8			7	70	100
9			24	50	85 <sup>d</sup>
10			24	45	76 <sup>e</sup>
11			1	99	100
12			1	99	100

<sup>a</sup>Reaction conditions: alcohol (1 mmol), catalyst (20 mg), H<sub>2</sub>O<sub>2</sub> (5 mmol), 70 °C.

<sup>b</sup>Yields are referring to isolated yields.

<sup>c</sup>Selectivity was based on the corresponding aldehydes or ketones.

<sup>d</sup>The byproduct is phenylacetic acid.

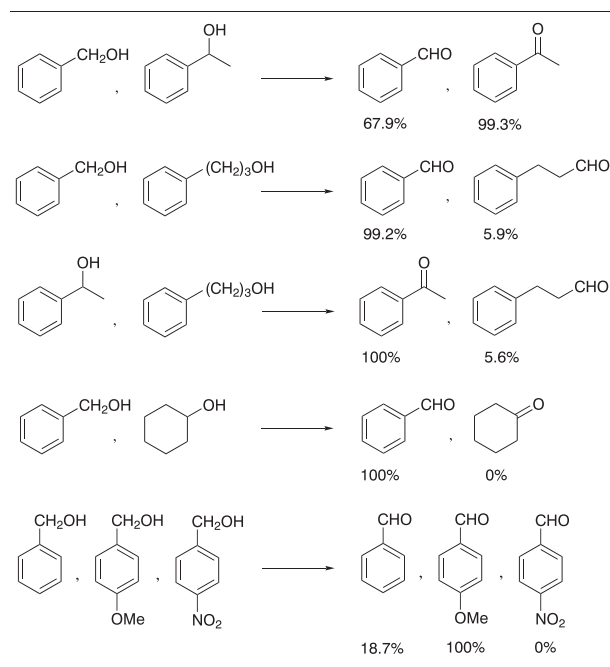
<sup>e</sup>The byproduct is 3-Phenylpropanoic acid.

oxidation of alcohols to corresponding aldehydes or ketones differs drastically.

In this context, we found that substituted benzyl alcohols bearing either electron-releasing or electron-withdrawing groups were also oxidized selectively and afforded the corresponding aldehydes in excellent to good yields under the optimized reaction conditions (Table 1, entries 1-7). For instance, 4-methoxybenzyl alcohol was converted into its corresponding aldehyde with 100% yield after 1.5 h while for 4-nitrobenzyl alcohol only 90% of its corresponding aldehyde was produced after 7 h (Table 1, entries 2, 6) without any over-oxidation to the corresponding carboxylic acid. 2-nitrobenzyl alcohol, a relatively hindered substrate was also converted to the corresponding aldehyde in good yields (70%) (Table 1, entry 5). The selective oxidation of 2-phenylethanol and 2-phenyl-1-propanol as models for challenging primary aliphatic alcohols was achieved in moderate yields (50% and 45%, respectively) and byproducts being their corresponding carboxylic acids. Secondary aromatic alcohols, such as 1-phenylethanol, and 1-phenyl-1-propanol were also converted to the corresponding ketones under the described reaction conditions with excellent yield (Table 1, entries 10 and 11). All our efforts for homoselective oxidation of 1,4-phenylenedimethanol failed and a mixture of mono- and dicarbonyl products were obtained (Table 1, entry 8).

To verify the chemoselectivity, a series of competition experiments were performed. An equimolar mixture of two or three types of alcohols was subjected to oxidation in the presence of GO/Fe<sub>3</sub>O<sub>4</sub>/HPW nanocomposite under optimized reaction conditions. Compared with primary aliphatic alcohols, the results revealed that 1° and 2° benzylic alcohols are more rapidly oxidized. When a 1:1 mixture of benzyl alcohol and 3-phenylpropanol was subjected to oxidation, benzaldehyde was produced in 99.2% yield and only 5.9% of 3-phenylpropanaldehyde was detected. Cyclohexanol as a 2° aliphatic alcohol remained intact in the course of oxidation so that when a mixture of cyclohexanol and benzyl alcohol was subjected to oxidation, only benzaldehyde was detected in 100% yield. Other competitive reactions were also performed and the results are summarized in Scheme 3. These results clearly indicate that this method can be used to oxidize benzyl alcohol in the presence of primary and secondary alcohols.

This high catalytic activity of GO/Fe<sub>3</sub>O<sub>4</sub>/HPW exhibited in the oxidation of alcohols can be attributed to high Bronsted acidity and acid content, synergetic catalytic effect, excellent surface activity and good solubility in water.<sup>[5,43,45]</sup> H<sub>2</sub>O<sub>2</sub> was activated by the GO/Fe<sub>3</sub>O<sub>4</sub>/HPW nanocomposite and then reacted with the heteropolyanion to generate active peroxy intermediate, and this active intermediate was responsible for the



**SCHEME 3** Chemoselective oxidation of an equimolar mixture of alcohols in the presence of GO/Fe<sub>3</sub>O<sub>4</sub>/HPW nanocomposite [Reaction conditions: Cat. (20 mg), H<sub>2</sub>O<sub>2</sub> (10%, 5 mmol), 70 °C, 3 h]

oxidation of alcohol to the corresponding aldehyde, ketone or carboxylic acid.<sup>[60,61]</sup>

The catalytic activity of GO/Fe<sub>3</sub>O<sub>4</sub>/HPW in the benzyl alcohol oxidation with hydrogen peroxide was compared with a few previous similar catalytic systems and summarized in Table 2. The results show that this new catalytic system is comparable or superior to some previous reports and has higher yield, shorter reaction time, milder reaction conditions, uses retrievable and reusable catalyst and avoids the use of toxic and volatile organic solvents.

### 3.9.4 | Recyclability of the catalyst

The recyclability of the heterogeneous catalyst is of paramount importance and has a critical advantage over homogeneous counterparts. Therefore, the recyclability of GO/Fe<sub>3</sub>O<sub>4</sub>/HPW nanocomposite was studied for the oxidation of benzyl alcohol under optimized reaction conditions (Figure 11). After each run, the catalyst was isolated from the reaction mixture by an external magnet, and then washed twice with ethanol and subsequently dried under vacuum. GO/Fe<sub>3</sub>O<sub>4</sub>/HPW can be reused five times without significant loss in conversion and selectivity.

The quantitative leaching out of active species of HPW from the support, before and after the reaction was evaluated by ICP analysis. According to the amount of Fe, Si, and W elements, it was found that the amounts of HPW washed out after the fifth run of the reaction was just

**TABLE 2** Comparison of the catalytic activity of GO/Fe<sub>3</sub>O<sub>4</sub>/HPW with some previous catalytic systems in the benzyl alcohol oxidation with H<sub>2</sub>O<sub>2</sub>

Entry	Catalyst	Reaction conditions	Yield (%)	Ref.
1	K <sub>11</sub> [Pr(PW <sub>11</sub> O <sub>39</sub> ) <sub>2</sub> ].xH <sub>2</sub> O	Cat. (0.24 mol%), alcohol (2 mmol), H <sub>2</sub> O <sub>2</sub> (4 mmol), H <sub>2</sub> O (0.4 ml), 90 °C, 3 h	70	4
2	[PZnMo <sub>2</sub> W <sub>9</sub> O <sub>39</sub> ] <sup>5-</sup> @APIB-MWCNT MWCNT = multi-wall carbon nanotubes APIB = 1-(3-aminopropyl)-3-butylimidazolium	Cat. (50 mg, 0.004 mmol), alcohol (0.5 mmol), H <sub>2</sub> O <sub>2</sub> (5 mmol), CH <sub>3</sub> CN (3 mL), reflux, 4 h	95	11
3	H <sub>3</sub> PW <sub>12</sub> O <sub>40</sub> -IL-SBA-15 IL = 1-(3-silylpropyl)-3-methylimidazolium	Cat. (100 mg), alcohol (5 mmol), H <sub>2</sub> O <sub>2</sub> (15 mmol), H <sub>2</sub> O (5.0 ml), 100 °C, 6 h	98	12
4	Fe <sub>3</sub> O <sub>4</sub> @SiO <sub>2</sub> /NH-PW <sub>10</sub> V <sub>2</sub> O <sub>40</sub>	Cat. (20 mol%, 0.02 g), alcohol (1.0 mmol), H <sub>2</sub> O <sub>2</sub> (2 ml), toluene (2 ml), 80 °C, 8 h	98	13
5	[DPyAM] HPW <sub>12</sub> O <sub>40</sub> <sup>2-</sup> DPyAM=N,N'-bis-2-aminoethyl-4,4'-bipyridinium	Cat. (0.1 g), alcohol (10 mmol), H <sub>2</sub> O <sub>2</sub> (30%, 6 mmol), 90 °C, 0.5 h	93	15
6	[TMGHA] <sub>2.4</sub> H <sub>0.6</sub> PW <sub>12</sub> O <sub>40</sub> TMGHA = N''-(3-amino-2-hydroxypropyl)-N,N',N',N'-tetramethylguanidinium	Cat. (0.03 mmol), alcohol (10 mmol), H <sub>2</sub> O <sub>2</sub> (30%, 15 mmol), H <sub>2</sub> O (6 ml), 90 °C, 6 h	91	17
7	[n-C <sub>16</sub> H <sub>33</sub> N(CH <sub>3</sub> ) <sub>3</sub> ] <sub>3</sub> PW <sub>12</sub> O <sub>40</sub>	Cat. (25 μmol), alcohol <sup>a</sup> (15 mmol), H <sub>2</sub> O <sub>2</sub> (27.5%, 10 mmol), 90 °C, 6 h	95	43
8	[(C <sub>18</sub> H <sub>37</sub> ) <sub>2</sub> (CH <sub>3</sub> ) <sub>2</sub> N] <sub>10</sub> [SiW <sub>9</sub> O <sub>34</sub> ]	Cat. (12 μmol), alcohol (2 mmol), H <sub>2</sub> O <sub>2</sub> (2 mmol), 65 °C, 6 h	47	45
9	S <sub>4</sub> [H <sub>4</sub> SiW <sub>12</sub> O <sub>40</sub> ] S=N-dodecyl-N,N-dimethyl-3-ammonio-1-propanesulfonate	Cat. (0.05 mmol), alcohol (30 mmol), H <sub>2</sub> O <sub>2</sub> (45 mmol), 70 °C, 4 h	94	47
10	[(N-butylpyridinium) <sub>4</sub> W <sub>10</sub> O <sub>32</sub> ]	Cat. (0.06 mmol), alcohol (50 mmol), H <sub>2</sub> O <sub>2</sub> (30%, 125 mmol), 80 °C, 8 h.	87	49
11	[bmim] <sub>5</sub> [PW <sub>11</sub> ZnO <sub>39</sub> ].3H <sub>2</sub> O	Cat. (0.05 mmol), alcohol (1 mmol), H <sub>2</sub> O <sub>2</sub> (10 mmol), CH <sub>3</sub> CN (3 ml), reflux, 1.25 h	100	51
12	Polypyridinium phosphotungstate	Cat. (0.02 mmol), alcohol (1 mmol), H <sub>2</sub> O <sub>2</sub> (30%, 6 mmol), t-BuOH (3 ml), 80 °C, 12 h	98 <sup>a</sup>	52
13	PW-NH <sub>2</sub> -IL-SBA-15	Cat. (0.1 g), alcohol (10 mmol), 100 °C, H <sub>2</sub> O <sub>2</sub> /alcohol (3:1), 6 h	92 <sup>b</sup>	53
14	Dendritic phosphotungstate hybrid (PW-PAMAM-G2)	Cat. (1.5 mol%), alcohol (10 mmol), H <sub>2</sub> O (1.5 ml), H <sub>2</sub> O <sub>2</sub> (30 wt.%, 15 mmol), 100 °C, 6 h	89 <sup>b</sup>	54
15	(PMo <sub>11</sub> Co) Co-substituted Keggin phosphomolybdate	Cat. (20 mg), H <sub>2</sub> O <sub>2</sub> /alcohol (3:1), 90 °C, 24 h	56 <sup>b</sup> (91) <sup>c</sup>	55
16	mesoporous Cr <sub>2</sub> O <sub>3</sub> -PWA composite	Cat. (0.008 mmol), alcohol (0.08 mmol), H <sub>2</sub> O <sub>2</sub> (30%, 4 equiv.), CH <sub>3</sub> CN (2 ml), 50 °C, 1 h	83 <sup>a</sup>	56
17	Cu <sub>1.00</sub> Fe <sub>1.00</sub> SiW <sub>11</sub> with graphite calcined at 350 °C	Cat. (10 mg), alcohol (0.43 g), H <sub>2</sub> O <sub>2</sub> /alcohol (5:1), toluene (5 ml), 80 °C, 1 h	98 <sup>b</sup> (98.3) <sup>c</sup>	57
18	VHPW/MCM-41/NH <sub>2</sub>	Cat. (0.05 g), alcohol (4 mmol), H <sub>2</sub> O <sub>2</sub> /alcohol (5:1), toluene (5 ml), 80 °C, 8 h.	93 <sup>b</sup> (100) <sup>c</sup>	58
19	GO/Im-PW <sub>12</sub> O <sub>40</sub> <sup>3-</sup> Im = 1-(3-silylpropyl)-3-methylimidazolium	Cat. (0.6 g), alcohol (40 mmol), H <sub>2</sub> O <sub>2</sub> (100 mmol), 90 °C, 7 h	90 (99) <sup>c</sup>	59
20	GO/Fe <sub>3</sub> O <sub>4</sub> /HPW	Cat. (20 mg), alcohol (1 mmol), H <sub>2</sub> O <sub>2</sub> (10%, 5 mmol), 70 °C, 3 h	99 (100) <sup>c</sup>	-

<sup>a</sup>1-Phenylethanol;<sup>b</sup>Conversion (%);<sup>c</sup>Selectivity (%).

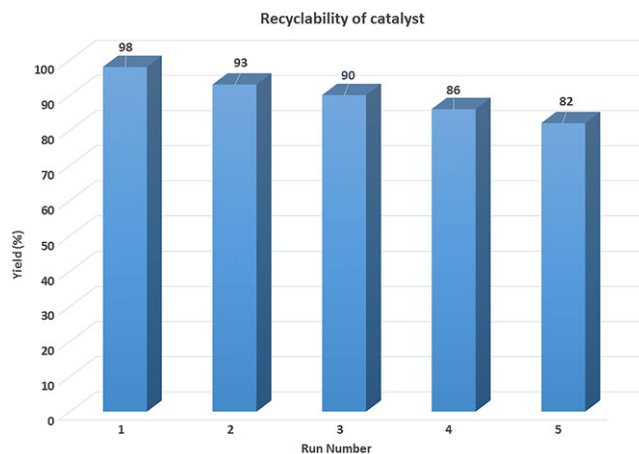


**FIGURE 11** Recyclability of GO/Fe<sub>3</sub>O<sub>4</sub>/HPW nanocomposite in the oxidation reaction of benzyl alcohol

1.6 %. Furthermore, in order to qualitatively test for leaching and heterogeneity, the oxidation reaction of benzyl alcohol to benzaldehyde was performed in the presence of GO/Fe<sub>3</sub>O<sub>4</sub>/HPW under optimized reaction conditions. After 1.5 h (t/2), the catalyst was removed by using a magnet. The GC results showed that in the absence of the catalyst, the reaction was completely stopped. Therefore, it can be concluded that the active component of the catalyst was not leached out and catalysis is heterogeneous in nature. In other procedures, the five times reused catalyst was also studied by FT-IR spectroscopy (Figure 1, j) and EDX analysis (Figure ESI-19). The results of the EDX analysis confirmed the presence of the desired elements and the FT-IR spectrum showed the characteristic peaks of the primary catalyst. This confirmed that the prepared catalyst was remarkably stable under reaction conditions and in practice, HPW particles were only slightly leached out from the support.

## 4 | CONCLUSION

We have developed a new catalytic system which is robust, safe and magnetically recoverable. Graphene oxide/Fe<sub>3</sub>O<sub>4</sub>/phosphotungstic acid (GO/Fe<sub>3</sub>O<sub>4</sub>/HPW) was prepared by functionalization of GO with amino-functionalized Fe<sub>3</sub>O<sub>4</sub> (Fe<sub>3</sub>O<sub>4</sub>@SiO<sub>2</sub>-NH<sub>2</sub>) through amide bond formation and then decorated by HPW.

In this catalytic system, graphene oxide sheets were used as a suitable support because they have favorable properties such as high surface area, good chemical stability, sufficient thermal and mechanical stability and the presence of appropriate functional groups for the creation of covalent bonds with other catalyst components. The NH<sub>2</sub>-silicacoated magnetic nanoparticles have the ability to make strong covalent bonds with graphene oxide

layers, and at the same time, the amino groups have the capability to maintain HPA particles by creating suitable ionic bonds. The presence of HPA on the magnetic graphene oxide results in an active and stable catalytic system with a high surface area with the capability of easily separating and being reused. The catalytic activity was observed only in the presence of HPA and the magnetic graphene oxide layers were designed for heterogenization of HPA and improvement of the retrievability and reusability of the catalyst.

This magnetically modified nanohybrid displayed excellent performance as a heterogeneous catalyst in the selective oxidation of alcohols with aqueous H<sub>2</sub>O<sub>2</sub>. Our new catalytic system was found to be very effective towards the oxidation of primary and secondary benzylic alcohols to the corresponding aldehydes or ketones with almost 75-99% conversions, without any over-oxidation to acid (100% selectivity). The oxidation reaction was also performed for two types of primary aliphatic alcohol to the corresponding aldehyde. The product efficiency was less than that of benzylic alcohols (45 and 50%) due to over-oxidation to the corresponding carboxylic acid. TGA analysis showed that the thermal stability of the catalyst was much higher than graphene oxide. To verify the chemoselectivity, a series of competition experiments were also undertaken.

## ACKNOWLEDGEMENTS

The authors are grateful for the financial support of the University of Kurdistan and the Iranian Nanotechnology Initiative Council.

## ORCID

Kamal Amani  <http://orcid.org/0000-0001-8717-7893>

## REFERENCES

- [1] (a) T. Okuhara, N. Mizuno, M. Misono, *Adv. Catal.* **1996**, *41*, 113. (b) C. L. Hill, C. M. Prosser-McCarta, *Coor. Chem. Rev.* **1995**, *143*, 407. (c) N. Mizuno, M. Misono, *Chem. Rev.* **1998**, *98*, 199. (d) I. V. Kozhevnikov, *Chem. Rev.* **1998**, *98*, 171. (e) T. Okuhara, *Catal. Today* **2002**, *73*, 167. (f) M. N. Timofeeva, *Appl. Catal. A: Gen.* **2003**, *256*, 19. (g) D. L. Long, E. Burkholder, L. Cronin, *Chem. Soc. Rev.* **2007**, *36*, 105.
- [2] Y. Zhou, G. Chen, Z. Long, J. Wang, *RSC Adv.* **2014**, *4*.
- [3] E. Rafiee, S. Eavani, *RSC Adv.* **2016**, *6*, 46433. and the references cited therein
- [4] M. K. Saini, R. Gupta, S. Parbhakar, S. Singh, F. Hussain, *RSC Adv.* **2014**, *4*, 38446.
- [5] A. Dolbecq, E. Dumas, C. R. Mayer, P. Mialane, *Chem. Rev.* **2010**, *110*, 6009 and the references cited therein

- [6] X. Rozanska, P. Sautet, F. Delbecq, F. Lefebvre, S. Borshch, H. Chermette, J. M. Bassety, E. Grinenval, *Phys. Chem. Chem. Phys.* **2011**, *13*, 15955.
- [7] X. Aparicio-Angles, P. Miro, A. Clotet, C. Bo, J. M. Poblet, *Chem. Sci.* **2012**, *3*, 2020.
- [8] M. V. Vasylyev, R. Neumann, *J. Am. Chem. Soc.* **2004**, *126*, 884.
- [9] F. Shahbazi, K. Amani, *Catal. Commun.* **2014**, *55*, 57.
- [10] D. -Y. Zhang, M. -H. Duan, X. -H. Yao, Y. -J. Fu, Y. -G. Zu, *Fuel* **2016**, *172*, 293.
- [11] R. Hajian, Z. Alghour, *Chinese Chem. Lett.* **2017**, *28*, 971.
- [12] H. Zhao, L. Zeng, Y. Li, C. Liu, B. Hou, D. Wu, N. Feng, A. Zheng, X. Xie, S. Su, N. Yu, *Micropor. Mesopor. Mat.* **2013**, *172*, 67.
- [13] X. Dong, X. Zhang, P. Wu, Y. Zhang, B. Liu, H. Hu, G. Xue, *ChemCatChem* **2016**, *8*, 3680.
- [14] Y. Leng, J. Liu, P. Jiang, J. Wang, *RSC Adv.* **2012**, *2*, 11653.
- [15] Y. Leng, P. Zhao, M. Zhang, J. Wang, *J. Mol. Catal. A: Chem.* **2012**, *358*, 67.
- [16] A. Bordoloi, S. Sahoo, F. Lefebvre, S. B. Halligudi, *J. Catal.* **2008**, *259*, 232.
- [17] G. Chen, Y. Zhou, Z. Long, X. Wang, J. Li, J. Wang, *ACS Appl. Mater. Interfaces* **2014**, *6*, 4438.
- [18] Y. Liu, D. Yu, C. Zeng, Z. Miao, L. Dai, *Langmuir* **2010**, *26*, 6158.
- [19] T. Huang, Z. R. Xie, Q. Y. Wu, W. F. Yan, *Dalton Trans.* **2016**, *45*, 3958.
- [20] Y. Leng, J. Wang, D. Zhu, L. Shen, P. Zhao, M. Zhang, *Chem. Eng. J.* **2011**, *173*, 620.
- [21] R. Liu, S. Li, X. Yu, G. Zhang, S. Zhang, J. Yao, B. Keita, L. Nadjo, L. Zhi, *Small* **2012**, *8*, 1398.
- [22] J. M. Yoo, J. H. Kang, B. H. Hong, *Chem. Soc. Rev.* **2015**, *44*, 4835.
- [23] H. P. Cong, J. J. He, Y. Lu, S. H. Yu, *Small* **2010**, *6*, 169.
- [24] J. Abraham, K. S. Vasu, C. D. Williams, K. Gopinadhan, Y. Su, C. T. Cherian, J. Dix, E. Prestat, S. J. Haigh, I. V. Grigorieva, P. Carbone, A. K. Geim, R. R. Nair, *Nat. Nanotechnol.* **2017**, *12*, 546.
- [25] R. R. Nair, H. A. Wu, P. N. Jayaram, I. V. Grigorieva, A. K. Geim, *Science* **2012**, *335*, 442.
- [26] P. Z. Sun, K. L. Wang, H. W. Zhu, *Adv. Mater.* **2016**, *28*, 2287.
- [27] G. P. Liu, W. Q. Jin, N. P. Xu, *Chem. Soc. Rev.* **2015**, *44*, 5016.
- [28] R. K. Joshi, P. Carbone, F. C. Wang, V. G. Kravets, Y. Su, I. V. Grigorieva, H. A. Wu, A. K. Geim, R. R. Nair, *Science* **2014**, *343*, 752.
- [29] A. Akbari, P. Sheath, S. T. Martin, D. B. Shinde, M. Shaibani, P. Chakraborty Banerjee, R. Tkacz, D. Bhattacharyya, M. Majumder, *Nat. Commun.* **2016**, *7*, 10891.
- [30] V. Georgakilas, M. Otyepka, A. B. Bourlinos, V. Chandra, N. Kim, K. C. Kemp, P. Hobza, R. Zboril, K. S. Kim, *Chem. Rev.* **2012**, *112*, 6156.
- [31] T. Gan, C. Hu, Z. Chen, S. Hu, *Sensor. Actuat. B: Chem.* **2010**, *151*, 8.
- [32] Y. Sun, J. Tang, K. Zhang, J. Yuan, J. Li, D. M. Zhu, K. Ozawa, L. C. Qin, *Nanoscale* **2017**, *9*, 2585.
- [33] D. Yu, Y. Yang, M. Durstock, J. B. Baek, L. Dai, *ACS Nano* **2010**, *4*, 5633.
- [34] Q. Liu, Z. Liu, X. Zhang, N. Zhang, L. Yang, S. Yin, Y. Chen, *Appl. Phys. Lett.* **2008**, *92*, 223303.
- [35] Y. Liu, J. Zhou, X. Zhang, Z. Liu, X. Wan, J. Tian, T. Wang, Y. Chen, *Carbon* **2009**, *47*, 3113.
- [36] N. Karousis, S. P. Economopoulos, E. Sarantopoulou, N. Tagmatarchis, *Carbon* **2010**, *48*, 854.
- [37] Z. Liu, J. T. Robinson, X. Sun, H. Dai, *J. Am. Chem. Soc.* **2008**, *130*, 10876.
- [38] V. Chandra, J. Park, Y. Chun, J. Woo Lee, I. C. Hwang, K. S. Kim, *ACS Nano* **2010**, *4*, 3979.
- [39] Z. Geng, Y. Lin, X. Yu, Q. Shen, L. Ma, Z. Li, N. Pan, X. Wang, *J. Mater. Chem.* **2012**, *22*, 3527.
- [40] K. Singh, A. Ohlan, V. H. Pham, R. Balasubramanian, S. Varshney, J. Jang, S. H. Hur, W. M. Choi, M. Kumar, S. K. Dhawan, B.-S. Kongd, J. S. Chung, *Nanoscale* **2013**, *5*, 2411.
- [41] H. Li, S. Pang, S. Wu, X. Feng, K. Müllen, C. Bubeck, *J. Am. Chem. Soc.* **2011**, *133*, 9423.
- [42] M. Wu, X. Zhang, X. Su, X. Li, X. Zheng, X. Guan, P. Liu, *Catal. Commun.* **2016**, *85*, 66.
- [43] S. Zhang, G. Zhao, S. Gao, Z. Xi, J. Xu, *J. Mol. Catal. A: Chem.* **2008**, *289*, 22.
- [44] M. M. Heravi, V. Zadsirjan, K. Bakhtiari, H. A. Oskooie, F. F. Bamoharram, *Catal. Commun.* **2007**, *8*, 315.
- [45] Y. Ding, W. Zhao, Y. Zhang, B. Ma, W. Qiu, *Reac. Kinet. Mech. Cat.* **2011**, *102*, 85.
- [46] K. Kawamura, T. Yasuda, T. Hatanaka, K. Hamahiga, N. Matsuda, M. Ueshima, K. Nakai, *Chem. Eng. J.* **2016**, *285*, 49.
- [47] X. Li, R. Cao, Q. Lin, *Catal. Commun.* **2015**, *69*, 5.
- [48] A. Bordoloi, S. Sahoo, S. B. Halligudi, *Catal. Surv. Asia* **2013**, *17*, 132.
- [49] D. Liu, J. Z. Gui, F. Lu, Z. L. Sun, Y.-k. Park, *Catal. Lett.* **2012**, *142*, 1330.
- [50] Y. Leng, P. Jiang, J. Wang, *Catal. Commun.* **2012**, *25*, 41.
- [51] Z. Nadealian, V. Mirkhani, B. Yadollahi, M. Moghadam, S. Tangestaninejad, I. Mohammadpoor-Baltork, *J. Coord. Chem.* **2012**, *65*, 1071.
- [52] Y. M. A. Yamada, C. K. Jin, Y. Uozumi, *Org. Lett.* **2010**, *12*, 4540.
- [53] A. R. Tan, C. Liu, N. Feng, J. Xiao, W. Zheng, A. Zheng, D. Yin, *Micropor. Mesopor. Mat.* **2012**, *158*, 77.
- [54] Y. Chen, R. Tan, W. Zheng, Y. Zhang, G. Zhaoa, D. Yin, *Catal. Sci. Technol.* **2014**, *4*, 4084.
- [55] S. Pathan, A. Patel, *Appl. Catal. A: Gen.* **2013**, *459*, 59.
- [56] I. Tamiolakis, I. N. Lykakis, A. P. Katsoulidis, C. D. Malliakas, G. S. Armatas, *J. Mater. Chem.* **2012**, *22*, 6919.
- [57] X. Dong, C. Yu, D. Wang, Y. Zhang, P. Wu, H. Hu, G. Xue, *Mater. Res. Bull.* **2017**, *85*, 152.
- [58] X. Dong, D. Wang, K. Li, Y. Zhen, H. Hu, G. Xue, *Mater. Res. Bull.* **2014**, *57*, 210.

- [59] a) W. H. Zhang, J. J. Shen, J. Wu, X. Y. Liang, J. Xu, P. Liu, B. Xue, Y. X. Li, *Mol. Catal.* **2017**, *443*, 262. b) Y. Leng, J. Liu, P. Jiang, J. Wang, *RSC Adv.* **2012**, *2*, 11653. c) C. Li, J. Gao, Z. Jiang, S. Wang, H. Lu, Y. Yang, F. Jing, *Top. Catal.* **2005**, *35*, 169.
- [60] R. Noyori, M. Aokib, K. Sato, *Chem. Commun.* **1977**, 2003.
- [61] K. Kamata, K. Yonehara, Y. Sumida, K. Yamaguchi, S. Hikichi, N. Mizuno, *Science* **2003**, *300*, 964.
- [62] M. Rezaei, K. Amani, K. Darvishi, *Catal. Commun.* **2017**, *91*, 38.
- [63] M. Rezaei, K. Azizi, K. Amani, *Appl Organometal Chem.* **2017**, e4120.
- [64] W. S. Hummers, R. E. Offeman, *J. Am. Chem. Soc.* **1957**, *80*, 1339.
- [65] D. Luo, G. Zhang, J. Liu, X. Sun, *J. Phys. Chem. C* **2011**, *115*, 11327.
- [66] G. Xie, P. Xi, H. Liu, F. Chen, L. Huang, Y. Shi, F. Hou, Z. Zeng, C. Shao, J. Wang, *J. Mater. Chem.* **2012**, *22*, 1033.
- [67] L. Sun, S. Hu, H. Sun, H. Guo, H. Zhu, M. Liu, H. Sun, *RSC Adv.* **2015**, *5*, 11837.
- [68] K. H. Liao, A. Mittal, S. Bose, C. Leighton, K. A. Mkhoyan, C. W. Macosko, *ACS Nano* **2011**, *5*, 1523.
- [69] A. Alizadeh, M. M. Khodaei, M. Beygzadeh, D. Kordestani, M. Feyzi, *Bull. Korean Chem. Soc.* **2012**, *33*, 2546.
- [70] M. Masteri-Farahani, J. Movassagh, F. Taghavi, P. Eghbali, F. Salimi, *Chem. Eng. J.* **2012**, *184*, 342.
- [71] E. Rafiee, S. Eavani, *Green Chem.* **2011**, *13*, 2116.
- [72] I. V. Kozhevnikov, *Catal. Lett.* **1994**, *27*, 187.
- [73] T. T. Tung, J. F. Feller, T. Kim, H. Kim, W. S. Yang, K. S. Suh, *J. Polym. Sci. Pol. Chem.* **2012**, *50*, 927.
- [74] P. Lian, X. Zhu, S. Liang, Z. Li, W. Yang, H. Wang, *Electrochim. Acta* **2010**, *55*, 3909.
- [75] B. Xu, S. Yue, Z. Sui, X. Zhang, S. Hou, G. Cao, Y. Yang, *Energy Environ. Sci.* **2011**, *4*, 2826.
- [76] J. Gui, D. Liu, Z. Sun, D. Liu, D. Min, B. Song, X. Peng, *J. Mol. Catal. A: Chem.* **2010**, *331*, 64.

## SUPPORTING INFORMATION

Additional Supporting Information may be found online in the supporting information tab for this article.

**How to cite this article:** Darvishi K, Amani K, Rezaei M. Preparation, characterization and heterogeneous catalytic applications of GO/Fe<sub>3</sub>O<sub>4</sub>/HPW nanocomposite in chemoselective and green oxidation of alcohols with aqueous H<sub>2</sub>O<sub>2</sub>. *Appl Organometal Chem.* 2018;e4323. <https://doi.org/10.1002/aoc.4323>